energies

MDPI

Review

Review of Key Technologies of the High-Speed Permanent Magnet Motor Drive

Quntao An [1,2,*], Yuzhuo Lu [1,*] and Mengji Zhao [1]

[1] School of Electrical Engineering and Automation, Harbin Institute of Technology, Harbin 150001, China; 23b906003@stu.hit.edu.cn
[2] State Key Laboratory of Hydro-Power Equipment, Harbin 150001, China
* Correspondence: anquntao@hit.edu.cn (Q.A.); 22b906047@stu.hit.edu.cn (Y.L.)

Abstract: The high-speed permanent magnet motor has been widely used in the industrial field because of its high-power density, fast dynamic response, and wide speed range. High efficiency and stable operation are the premises for the high-speed permanent magnet motor to exert its advantages. Firstly, this article analyzes the problems existing in the drive technology of high-speed permanent magnet motors from three aspects: current harmonics, rotor position detection, and low carrier ratios. Aiming to address the above problems, the status of the latest research is summarized from the aspects of harmonic suppression, position sensorless, and control strategies. In addition, future research trends for high-speed permanent magnet motors are discussed.

Keywords: high-speed permanent magnet motor (HS PMM); drive technology; harmonic suppression; rotor position detection; control strategy; decoupling control; delay compensation

1. Introduction

The common requirement of high-speed motors is that their speed is more than 10,000 r/min or the product of speed and the square root of power exceeds 1×10^5. High-speed motors are widely used in electric vehicles, fans, compressors, and microturbines because of their high-power density, high efficiency, and wide-speed operation [1–4]. At present, induction motors [5], switched reluctance motors [6] and permanent magnet motors [7] have been used on high-speed occasions. In the above applications, the complexity and redundancy of the HS PMM system are greatly reduced, so that it has high-power factor and efficiency. Therefore, HS PMMs have important academic research significance and value. Darmstadt University of Technology in Germany has developed a HS PMM with a speed of 40,000 r/min, and the carbon-fiber bandage is used to hold permanent magnets in place, which increases the mechanical strength of the motor [8]. Eth Zurich has developed a magnetic levitation HS PMM with a speed of 550,000 r/min, which was used in a gas turbine [9]. In South Korea, Chungnam National University developed a 12,500 r/min HS PMM, which is applied in a centrifugal pump system [10]. In addition, in China, Shenyang University of Technology designed a prototype of 18,000 r/min/1.12 MW HS PMM [11]. Southeast University designed a new type of permanent magnet motor with 18,000 r/min [12]. The mechanical, electromagnetic, and anti-demagnetization properties of surface-mounted permanent magnet (SPM) motors and interior permanent magnet (IPM) motors are compared in [13]. By comparison, the cost and torque of the SPM motor are superior to the IPM motor. However, the rotor structure of the SPM motor is not robust enough, and it is prone to irreversible demagnetization. Due to the HS PMM being mostly used in precision fields, its design and drive are required to be more rigorous. When the speed of motors is high, the increased high-frequency eddy current loss will lead to more severe rotor heating [14,15]. Therefore, the design of HS PMMs cannot follow traditional methods, structures, and materials, and loss and temperature rise must seriously be taken into account.

check for updates

Citation: An, Q.; Lu, Y.; Zhao, M. Review of Key Technologies of the High-Speed Permanent Magnet Motor Drive. *Energies* **2024**, *17*, 5252. https://doi.org/10.3390/en17215252

Academic Editor: Ahmed Abu-Siada

Received: 21 July 2024
Revised: 9 September 2024
Accepted: 16 October 2024
Published: 22 October 2024

Copyright: © 2024 by the authors. Licensee MDPI, Basel, Switzerland. This article is an open access article distributed under the terms and conditions of the Creative Commons Attribution (CC BY) license (https://creativecommons.org/licenses/by/4.0/).

In terms of the HS PMM drive, due to the inductor of HS PMMs being small, a lot of high-frequency noises will be generated. Therefore, the motor currents contain abundant high-frequency harmonic components. Extra losses, torque ripples, and operation noises are caused by current harmonics, and the stability performance of the system will be greatly weakened. The traditional drive technology is prone to cause system instability or even damage, and it fails to comply with the requirements of the HS PMM system [16,17]. Secondly, the position of the rotor is difficult to measure directly with sensors when the motor runs at a high speed. As a result, the stability and reliability of the whole system will be reduced [18]. Finally, owing to the elevated fundamental frequency of the motor, the switching frequency of the power device is constrained, resulting in a relatively low carrier ratio during high-speed operation. Therefore, the sine degree of the stator current gets worse, and the current harmonics increase significantly [19]. Moreover, the delay effect caused by the motor drive with low carrier ratios can be aggravated [20].

An efficient and stable drive system is a premise for the highly efficient operation of HS PMMs. In this paper, the technical difficulties of the harmonic suppression, rotor position detection, and control strategy of the HS PMM are first analyzed. Secondly, the latest research progress is reviewed. Finally, the developmental directions and research trends of HS PMMs are summarized and prospected.

2. Technical Difficulties of the HS PMM Drive

2.1. Harmonic Suppression

Air-gap magnetic field distortion of the motor body, nonlinear characteristics of the inverter, and a small inductor contribute to the significant generation of high-frequency harmonics in the motor phase current, and the current waveform distortion is serious. Due to the existence of harmonics, the motor losses are increased and the heating is serious; at the same time, torque and speed ripples will be generated, and the stability of the motor operation is affected [21,22]. Therefore, how the current harmonics are suppressed is extremely important.

2.2. Rotor Position Detection

To effectively control the HS PMM, it is essential to acquire precise rotor position information. Traditionally, mechanical sensors are installed on the rotating shaft to detect the position of the rotor [23]. However, mechanical sensors increase the size and cost of the HS PMM system, reducing the stability of the system. In order to overcome the above-mentioned problems, sensorless technologies in the HS PMM drive system have been widely studied. However, under high-speed conditions, the sensorless algorithm is affected by the nonlinear characteristics of the inverter and inconsistent motor parameters, which leads to the increased difficulty of rotor position estimation [24,25]. Therefore, regarding the drive system, the accuracy of rotor position detection has become of considerable interest.

2.3. System Stability under Low Carrier Ratios

The fundamental frequency of HS PMMs is more than 1 kHz, while the switching frequency is usually about 10 kHz, which makes the carrier ratio of the system even lower than 10. However, the modulation and control delay of the motor drive will be increased under the low carrier ratio condition, and the stability of the close-loop control is affected. In addition, the HS PMM drive system will develop the serious coupling phenomenon of flux linkage and torque [26,27]. These problems will cause system instability.

To sum up, the design of HS PMM drive systems is a strict process. Many factors need to be considered, such as harmonic suppression, rotor position detection, and the system control strategy, as shown in Figure 1. Therefore, the system has extremely high requirements and standards for these control objectives.

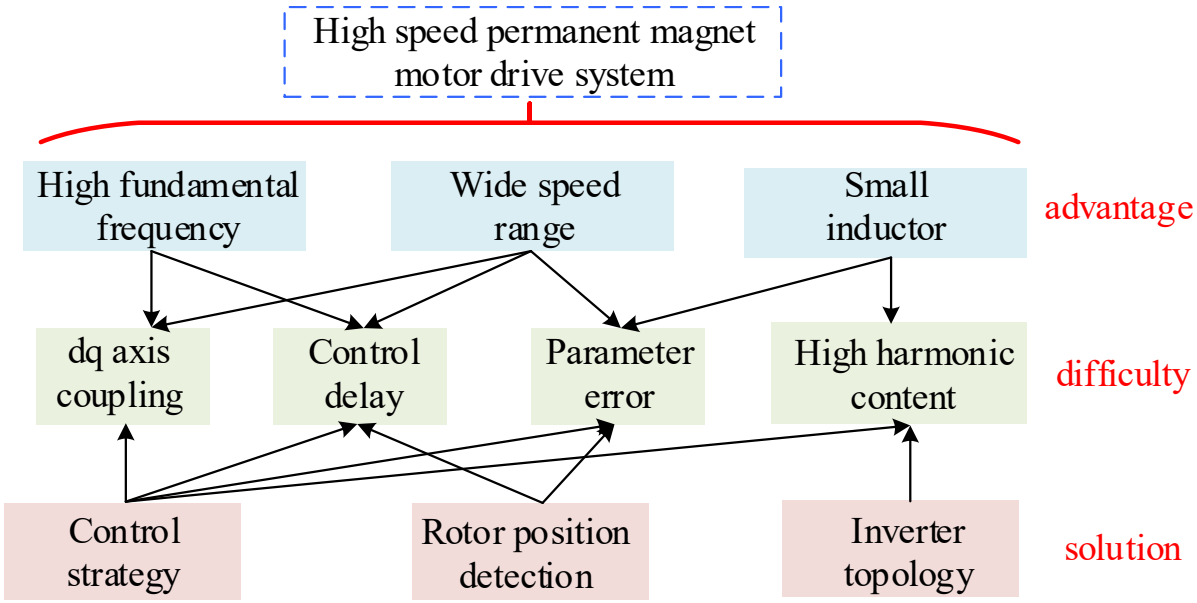


Figure 1. Drive system design difficulties and solutions.

3. Harmonic Suppression Schemes for HS PMMs

The fundamental frequency of HS PMMs is rather high, but the switching frequency of the inverters is limited. Therefore, the carrier ratio is relatively low with high-speed operation, which makes the current waveforms worse. In addition, the inductances of the HS PMM are small, which will result in a large number of high-frequency harmonics in the motor currents. At present, the methods for suppressing harmonics include adding inverter output filters, increasing the switching frequency, and improving the topology of the inverter.

3.1. Inverter Output Filter

In order to suppress the current harmonics, the inductor–capacitor–inductor (LCL)-type filter can be installed in the HS PMM system. The filter has a low-pass characteristic, so the current harmonics can be reduced and current waveforms can be improved. However, with an increase in the system power, the volume and weight of the filter also increase. Therefore, in order to reduce its weight, the structural design of the filter has been studied extensively [28,29].

Although the LCL filter can reduce harmonic components, it will result in a resonance problem. The resonance can not only cause current oscillations near the cut-off frequency but also endanger the stability of the control system. As shown in Figure 2, to suppress LCL resonance, an active damping control strategy based on the capacitor current is designed [30]. The experimental results show that the strategy is effective in suppressing LCL resonance within the Nyquist frequency. In Figure 2, i_{sA}~i_{sC} represents the stator currents; i_{nA}~i_{nC} is the filter capacitor currents; θ_e is the electrical angle of the motor; n_{ref} and n refer to the given and actual speed of the motor, respectively; i^*_{sdq} and i_{sdq} represent the given and actual current with complex vector form, respectively; i_{ndq} is the capacitor current with complex vector form; u^*_{wdq} is the output voltage of the inverter; and $G_a(z)$ and $G_b(z)$ are active damping controllers.

On this basis, in order to dispose of voltage sensors, the active damping control strategy based on motor current feedback and the notch filter is also studied [31,32].

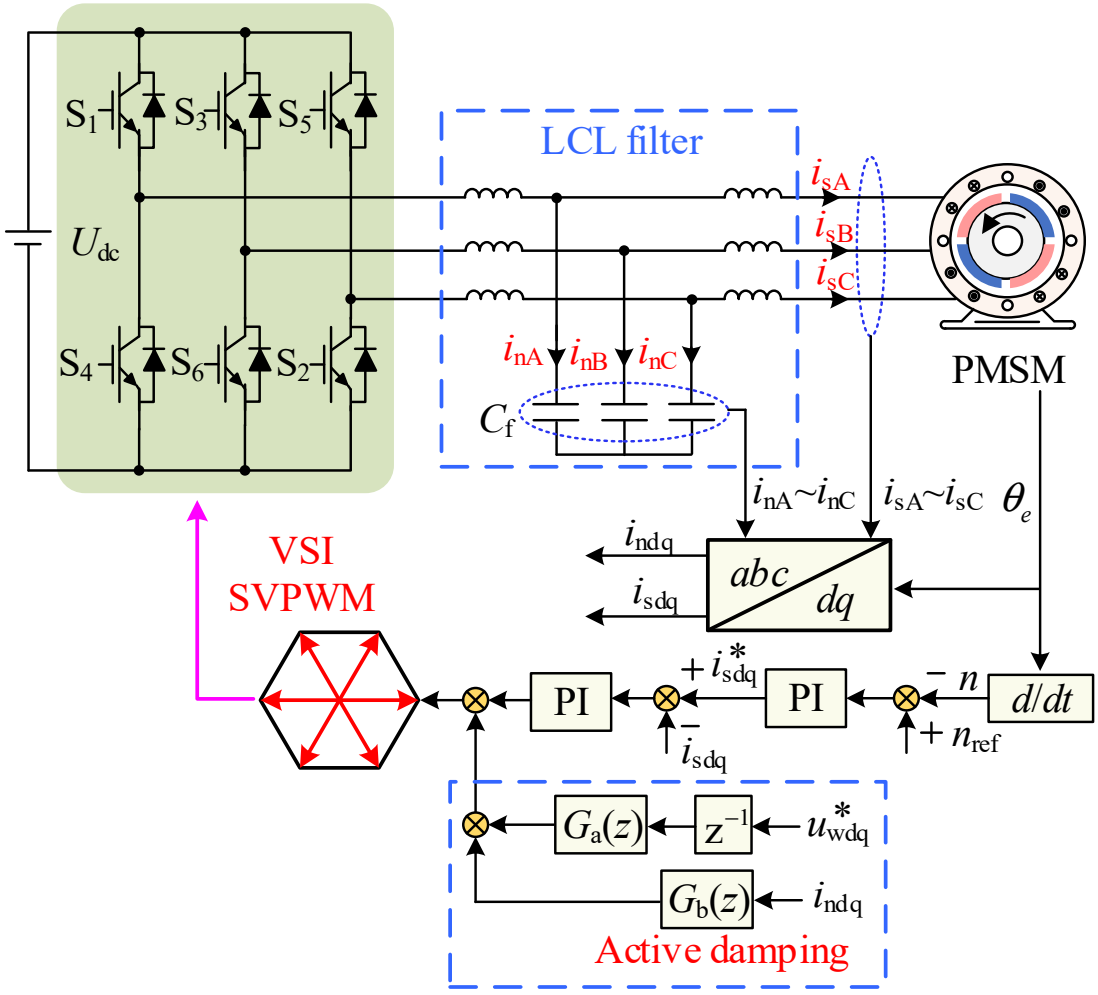


Figure 2. Active damping control system in [30].

3.2. Increased Switching Frequency

The most direct way of increasing the switching frequency is to use the wide bandgap semiconductor device. Due to the small on-resistance and low switching loss, SiC and GaN devices are being used [33]. For GaN devices, the device power rating is lower (less than 900 V and 150 A). However, for SiC devices, commercial device power ratings can be achieved up to 3.3 kV and 800 A. As a result, SiC devices are more suitable for motor drive applications [34]. According to the latest research, SiC nanowires and perovskite FETs can further improve the performance of SiC devices [35]. To show the advantages of SiC-MOSFET, the characteristics of Si-MOSFET, Si-IGBT, and SiC-MOSFET are summarized in Table 1 [36,37].

Table 1. Characteristics of Si-MOSFET, Si-IGBT, and SiC-MOSFET.

Characteristic	Si-MOSFET	Si-IGBT	SiC-MOSFET
Rated voltage	20–650 V	>650 V	>650 V
Switching frequency	>20 kHz	5–20 kHz	>50 kHz
Drive voltage	0–15 V	10–20 V	25–30 V
Power level	<3 kW	>3 kW	>5 kW

In addition, numerical simulations of Si-IGBT and SiC-MOSFET are carried out [38]. The results show that the torque, speed ripple, and stator current harmonics of SiC-MOSFET are less than Si-IGBT. However, the fast switching speed of SiC-MOSFET will easily lead to high voltage surge spikes and changeling EMI problems [39,40]. In order to improve the

switching frequency and avoid serious EMI, high-speed motor drivers based on SiC and Si hybrid have become a primary focus of research [41].

3.3. Improved Inverter Topologies

3.3.1. Multilevel Inverters

Multilevel topologies have been widely used in high-power motor drives. The number of output levels is increased, output voltages close to sine waveforms can be obtained, and current harmonics can be reduced. Therefore, multilevel inverter topologies are also used in high-speed motor drives. At present, diode-clamped inverters, T-type inverters, flying-capacitor inverters, and active neutral-point-clamped inverters are usually used, as shown in Figure 3.

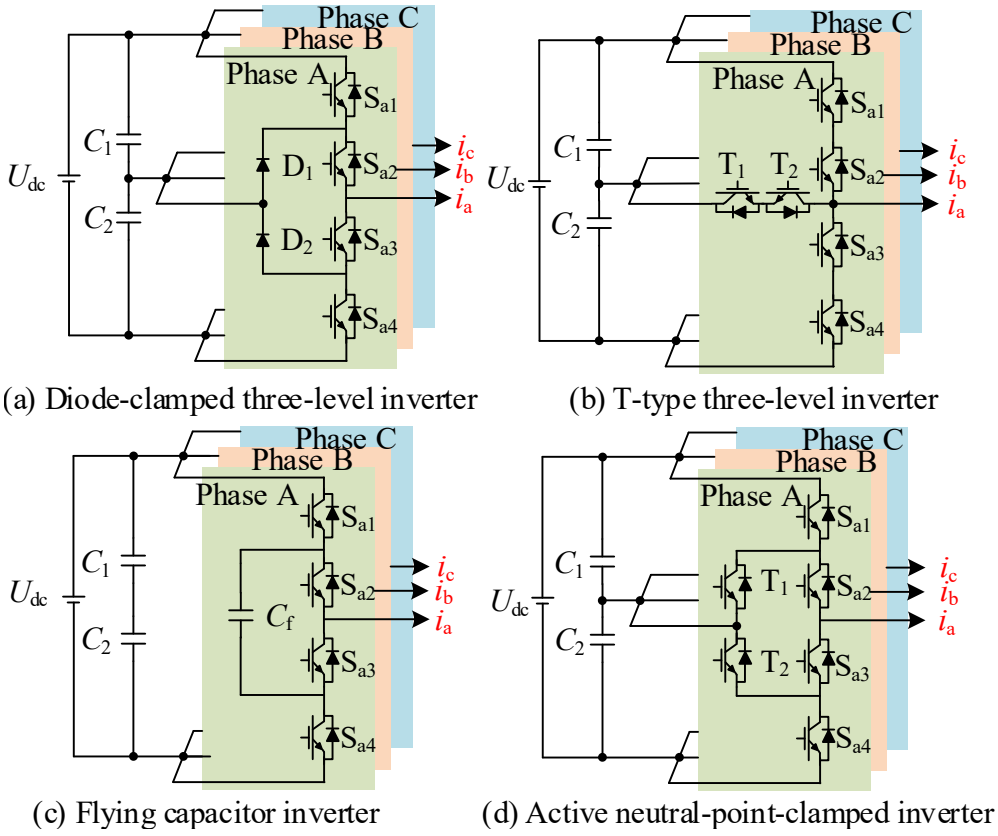


Figure 3. Topologies of multilevel inverter.

The output voltages of the diode-clamped inverter [42] and the T-type neutral-point-clamped inverter [43] have three levels of ±Vdc/2 and 0, and the problem of current ripple is alleviated. The flying-capacitor inverter [44] and the active neutral-point-clamped inverter [45] are also used to drive permanent magnet motors. In addition to the several topologies of multilevel inverters mentioned above, there are currently coupled-inductor three-level [46], five-level [47], and nine-level [48] inverters. While multilevel inverters can effectively mitigate the voltage stress on switches, the cost, volume, and switching losses of the system increase relative to the increase in the number of switches. However, due to the increase in the number of switches, the cost, volume, and switching loss of the system are relatively increased. Consequently, multilevel inverters are not suited for applications in integrated and cost-effective high-speed motor systems.

3.3.2. Inverters with DC Bus Voltage Regulation

The Z-source network [49], and the Buck converter [50] are commonly employed to regulate the DC bus voltage, thereby mitigating the current harmonics components, as

illustrated in Figure 4. Furthermore, the Z-source inverter can also raise the bus voltage to extend the motor speed range.

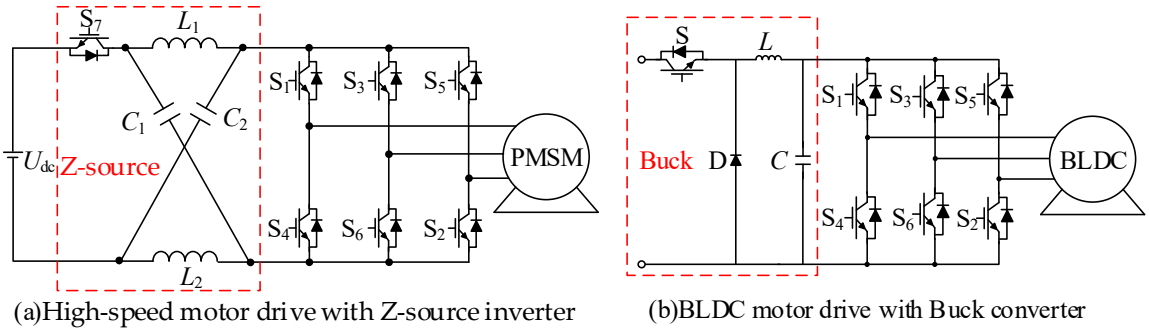


Figure 4. Inverters with DC bus voltage regulation.

As shown in Figure 4b, when brushless DC (BLDC) motors run at low speed, the Buck converter is employed to reduce the bus voltage for low current harmonics [51]. In [52], pulse width modulation (PWM) and pulse amplitude modulation (PAM) of the high-speed BLDC motor drive system are analyzed and compared, and the results show that the PAM control can effectively reduce high-frequency current harmonics. The current harmonics and losses of HS PMMs at low speeds can be reduced by the inverter with DC bus voltage regulation. But the loss at the rated power point cannot be decreased and a front-end DC converter with the same power is needed.

3.3.3. Current Source Inverter

The topology of the current source inverter (CSI) is shown in Figure 5. The CSI can directly output expected current waveforms, while the voltage source inverter (VSI) controls the current indirectly by adjusting the output voltage. The CSI only needs to ensure that the DC bus current is the amplitude of the winding current. Compared with the VSI, the CSI has the following advantages [53]:

(1) Better output waveforms: Output capacitors of the CSI and inductors of the motor constitute a CL filter. Therefore, the CSI can output sinusoidal voltages and currents.
(2) Boost ability: The VSI is a Buck topology, and the DC side voltage is higher than the AC side. However, the CSI is a Boost topology, which can obtain higher AC voltages. Therefore, the speed range of the motor can be extended.
(3) Short-circuit tolerant capacity: The CSI is fed by a constant current source, and the arm shoot-through state is permitted. Furthermore, the output short-circuit current can be suppressed by the constant current source.

The constant current source can be obtained indirectly by a combination of the voltage source and an inductor [54]. However, the energy feedback cannot be realized when the motor brakes. To solve this problem, the chopper circuit [53], the H-bridge converter [55], and the rectifier [56] are proposed to revise the topology.

The selective harmonic elimination (SHE), the trapezoidal pulse width modulation (TPWM), and the space-vector modulation (SVM) are the three main modulation strategies of the PWM CSI [57]. The SHE scheme has good harmonic elimination capacity, but it needs prior offline calculation and is not appropriate in high-dynamic situations. The TPWM is a carrier-based modulation scheme, and it demands a special trapezoidal modulation waveform design, which results in limited DC current utilization and poor output quality. The SVM is an online modulation strategy, which has good dynamic adjustment ability and wide modulation range, and can realize effective utilization of the DC bus current [58].

The second-order CL filter is composed of the inverter output capacitor and the motor inductor and can filter out high-frequency harmonics. However, it also introduces a resonance issue associated with the CL configuration. In order to suppress CL resonance, an active damping control strategy based on capacitor voltage feedback is proposed [59].

In [60], the voltage closed-loop controller is employed, as shown in Figure 6, to reduce system order and suppress the resonance peak. i_{wa}~i_{wc} refers to the three-phase current output by the CSI; u_A~u_C refers to three-phase voltage; i_{na}~i_{nc} is the current of the filter capacitors; i_{sA}~i_{sC} represents the three-phase current of the motor; θ_e is the electrical angular velocity; n_{ref} and n refer to the given and actual speed of the motor, respectively; i^*_{sdq} and i_{sdq} represent the given and actual current in the dq frame with complex vector form, respectively; and u^*_{sdq} and u_{sdq} are the given and actual voltage in the dq frame with complex vector form, respectively.

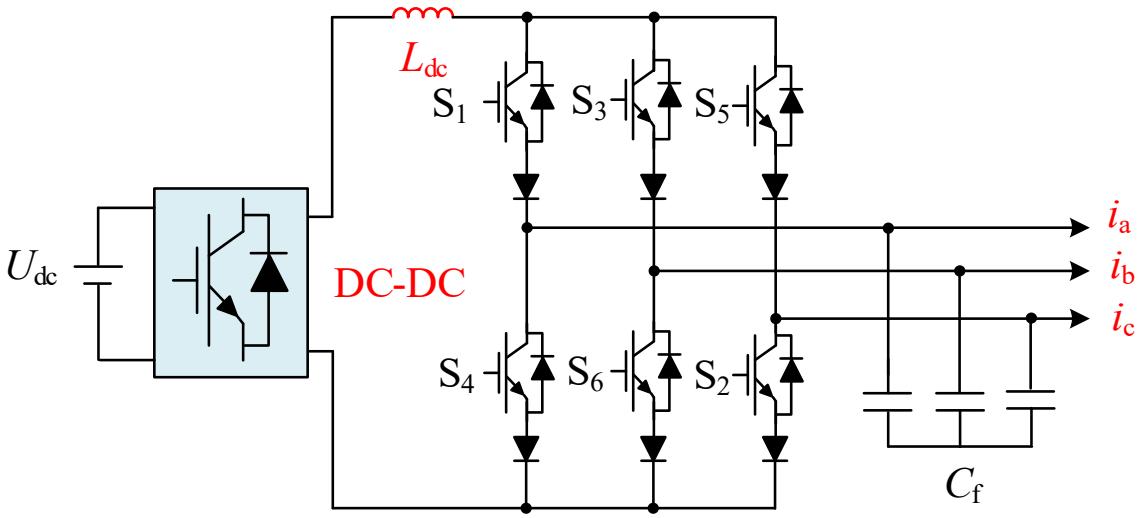


Figure 5. Current source inverter.

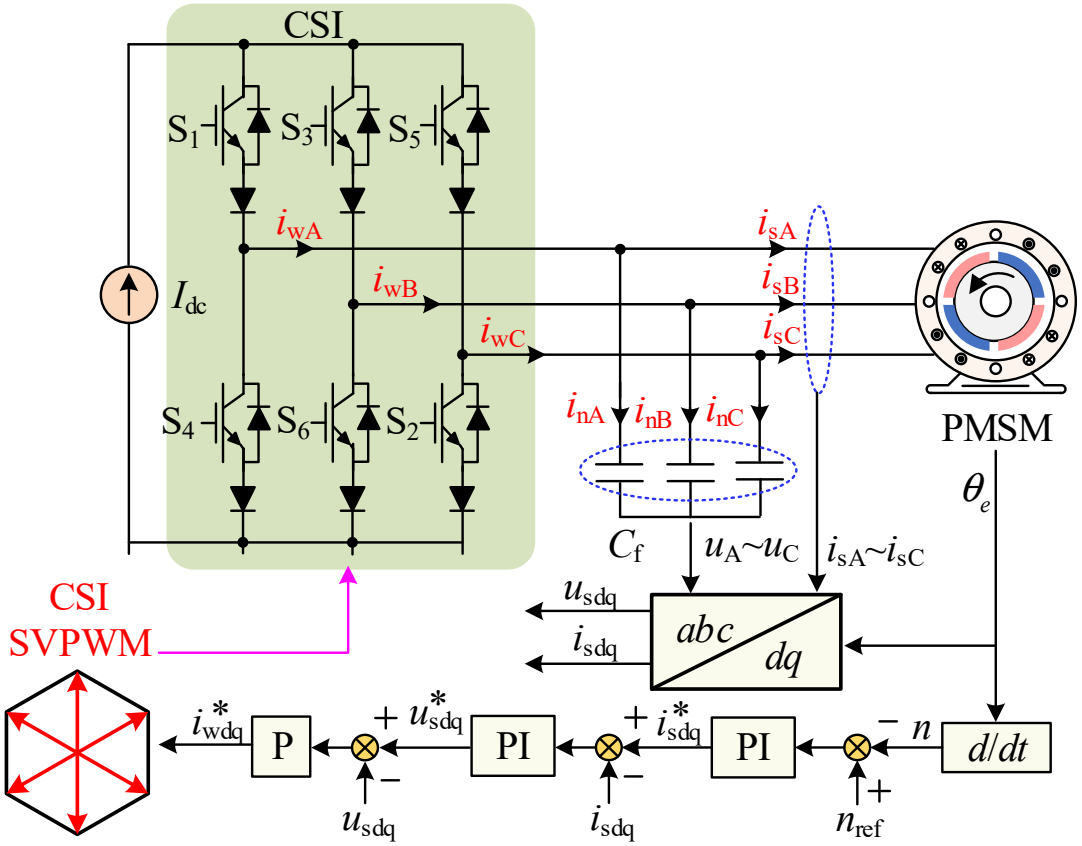


Figure 6. Control strategy of the high-speed PMSM fed by CSI in [60].

4. Rotor Position Detection of the HS PMM

Accurate rotor position information is essential for optimizing the high-performance control of HS PMMs. Rotor position detection is mainly divided into two methods: mechanical sensors and sensorless detection.

4.1. Mechanical Sensors

Resolvers [61], optical encoders [62], and Hall-effect sensors [63] are commonly used as position sensors in PMM drives. Nevertheless, resolvers and optical encoders exhibit limitations in high-speed motor applications due to constraints related to mechanical strength and frequency response. Hall sensors have simple structures that are divided into discrete and linear structures, and the discrete Hall sensors are commonly used in BLDC motors. The primary advantage of linear Hall sensors lies in their continuous signal output, which facilitates the extraction of positional information. In [64], a set of linear Hall sensors was installed at the stator slots of PMSMs to measure magnetic flux density in the time domain, effectively addressing the issue of rotor eccentricity. To effectively suppress harmonics during the operation of the HS permanent magnet motor (PMM), two linear Hall sensors are employed for rotor position detection, and a high-precision method based on synchronous frequency extraction is proposed in [65]. However, the application of mechanical sensors reduces the system's reliability. Therefore, sensorless algorithms are proposed for the HS PMM drive.

4.2. Sensorless Detection

Sensorless control of the HS PMM is divided into two categories, including the high-frequency injection (HFI) method and the back electromotive force (EMF) estimation method. The high-frequency injection method can work well in the range of zero speed and low speed, but fluctuations in current and torque will be caused by the injected high-frequency signals. The EMF estimation method uses the motor fundamental waveform model to estimate the EMFs, and then the EMFs can be used to extract position and speed information. Hence, these kinds of methods, including the Luenberger observer, the sliding mode observer (SMO), the extended Kalman filter (EKF), and the model reference adaptive system (MRAS), are effective under medium and high-speed conditions. In practice, it is recommended to combine the high-frequency injection method and the model-based method to achieve whole-speed range sensorless control. In [66], a hybrid seamless position tracking observer is used to estimate rotor position with smooth switching between the dual position tracking observer. The high-frequency injection method contributes to position estimation when the model-based position estimation method fails. When the speed is low, the position is dependent on the HFI method. Then, the weighting of the HFI method decreases as the speed increases, until a specific speed is reached.

4.2.1. Luenberger Observer

The Luenberger observer belongs to one of the state observers. It realizes the closed-loop correction ability of the observation value by feeding back the observation error of the output and uses eigenvalue assignment to obtain a fast convergence rate. In [67,68], single-dimension and full-order Luenberger observers were designed, respectively.

4.2.2. Sliding Mode Observer

The SMO is a variable structure state observer. In traditional SMO, the error between the estimated and measured stator current is selected as the sliding surface. The motor EMF is extracted by a Bang-Bang-based control function, which also ensures the finite-time convergence of the SMO. Therefore, the SMO has the advantages of strong robustness and a fast dynamic response. However, the traditional SMO has an inherent chattering problem. The application of the switching function will result in a continual switch from the ON and OFF state. Therefore, the saturation function and the high-order SMO were employed to suppress chattering in [69,70]. In order to reduce chattering and eliminate phase shift,

an enhanced SMO is proposed in [71]. This method uses a frequency adaptive complex coefficient filter (FACCF) to replace the low pass filter, which can extract back EMF without distortion. Its control block diagram is shown in Figure 7. u_α, u_β, i_α, i_β, e_α, and e_β are the voltages, currents, and back EMFs of axis α and axis β. ω and θ are the rotor electrical angular velocity and position, respectively. The symbol "^" represents estimated values, and z_α and z_β are sliding mode control functions. Compared to the traditional SMO, the FACCF-based SMO achieved good estimation performance when the switching frequency was reduced to 600 Hz.

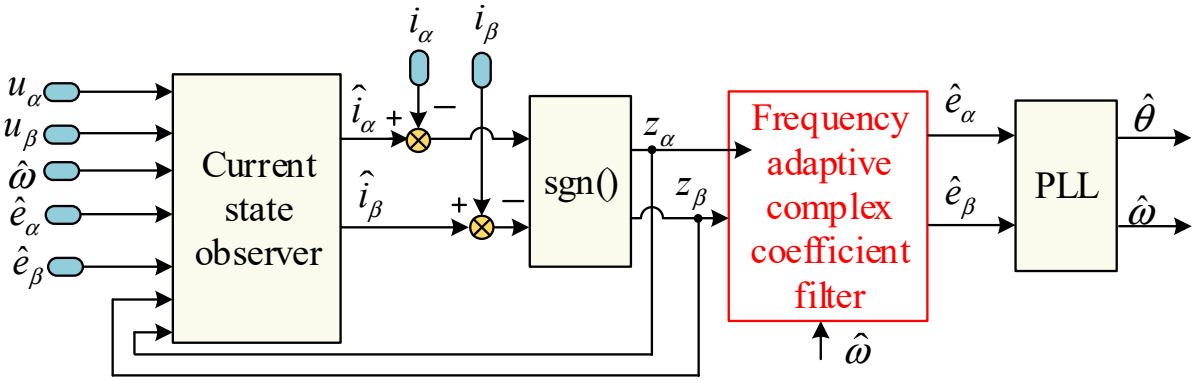


Figure 7. Position and speed estimation based on the SMO with FACCF.

4.2.3. Extended Kalman Filter

EKF is an optimal estimation method for linear systems containing only white noise, so it is widely used in the field of motor control. A reduced-order extended Kalman filter algorithm is proposed in [72]. By analyzing the characteristics of the system state matrix, the sensorless control of the PMSM based on third-order EKF velocity estimation is realized. In [73], an adaptive EKF is proposed. The process noise covariance matrix is updated online by calculating the scalar factor based on the residual sequence covariance matrix, which improves the adaptive ability of the system and the accuracy of speed estimation. However, this method needs a large amount of calculation and is sensitive to the motor parameter change.

4.2.4. Model Reference Adaptive System

The MRAS uses the plant as a reference model, and a model with unknown parameters, which is built according to the plant to be adjustable. When the same reference is input to the two models, an appropriate adaptive law is designed to adjust the model parameters according to the output errors. When the two models have the same outputs, the unknown parameters can be identified. An adaptive full-order observer is proposed in [74]. By introducing a correction segment, the method combines the estimation equation with the correction segment to form a closed-loop estimation. Moreover, the SMO is used instead of the traditional PI controller to control the speed loop, and the anti-interference ability of the system is improved.

5. Control Strategy with Low Carrier Ratios

5.1. System Stability Analysis with Low Carrier Ratios

The coupling and digital control delay of the HS PMM drive increase when it runs at high speed. In this case, the current loop is easy to lose control.

Figure 8a shows the mathematical model of the PMSM. R_s is the stator resistance, ψ_f is the permanent magnet flux, ω_e represents the electrical angular velocity, u_d and u_q are dq axis voltages, i_d and i_q are dq axis currents, and L_d and L_q are dq axis inductors.

Figure 8b shows the PMSM impedance coupling model. Equation (1) can be obtained through derivation as:

$$\begin{cases} Z_{dd}^{-1} = \frac{L_q s + R_s}{L_d L_q s^2 + L_d R_s s + L_q R_s s + L_d L_q \omega_e^2 + R_s^2} \\ Z_{dq}^{-1} = \frac{L_q \omega_e}{L_d L_q s^2 + L_d R_s s + L_q R_s s + L_d L_q \omega_e^2 + R_s^2} \\ Z_{qd}^{-1} = \frac{-L_d \omega_e}{L_d L_q s^2 + L_d R_s s + L_q R_s s + L_d L_q \omega_e^2 + R_s^2} \\ Z_{qq}^{-1} = \frac{L_d s + R_s}{L_d L_q s^2 + L_d R_s s + L_q R_s s + L_d L_q \omega_e^2 + R_s^2} \end{cases} \quad (1)$$

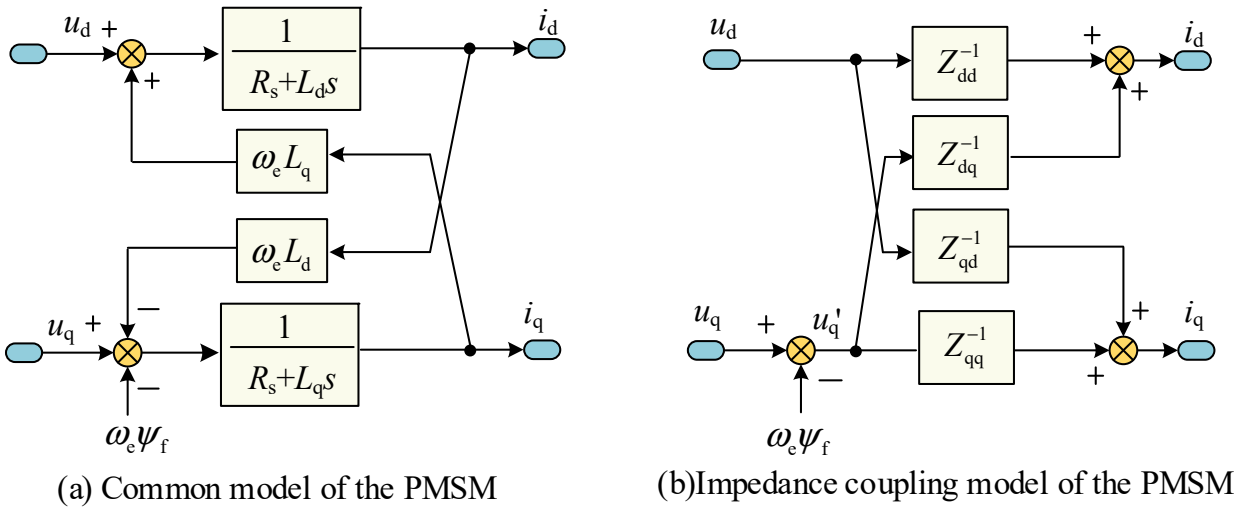


Figure 8. Mathematical model of the PMSM.

Under the steady-state ideal condition, the coupling terms Z_{dq} and Z_{qd} of the high-speed PMSM will be increased with increasing speed, and the coupling effect between the *dq* axes also increases. Therefore, to reduce the impact of the above two problems, it is essential to carry out accurate mathematical modeling of high-speed PMSMs and adopt the decoupling control strategy.

As for the BLDC motor square wave drives and PMSM sine wave drives, there are different decoupling strategies.

5.2. Square Wave Drive for BLDC Motors

The BLDC motor has back EMFs with trapezoidal waveforms, and its drive currents are square waveforms. At present, the common control methods are current-loop control and direct torque control (DTC). The current-loop control strategy has a large torque ripple when the motor runs at high speed. There are two kinds of DTC for high-speed BLDC motors, one is the DTC with torque and flux closed loops [75], and the other is the DTC without flux closed-loop control [76]. The second method can simplify the control structure, but the flexibility of the stator flux trajectory is reduced. Although the traditional current-loop control and DTC do not require complex coordinate transformations, the coupling problem of the HS PMM drive still exists. In addition, the square wave drive has a higher torque ripple than that of the sine wave drive, and the starting performance and magnetic weakness capability are also lower than the sine wave drive [77].

5.3. Sine Wave Drive for PMSMs

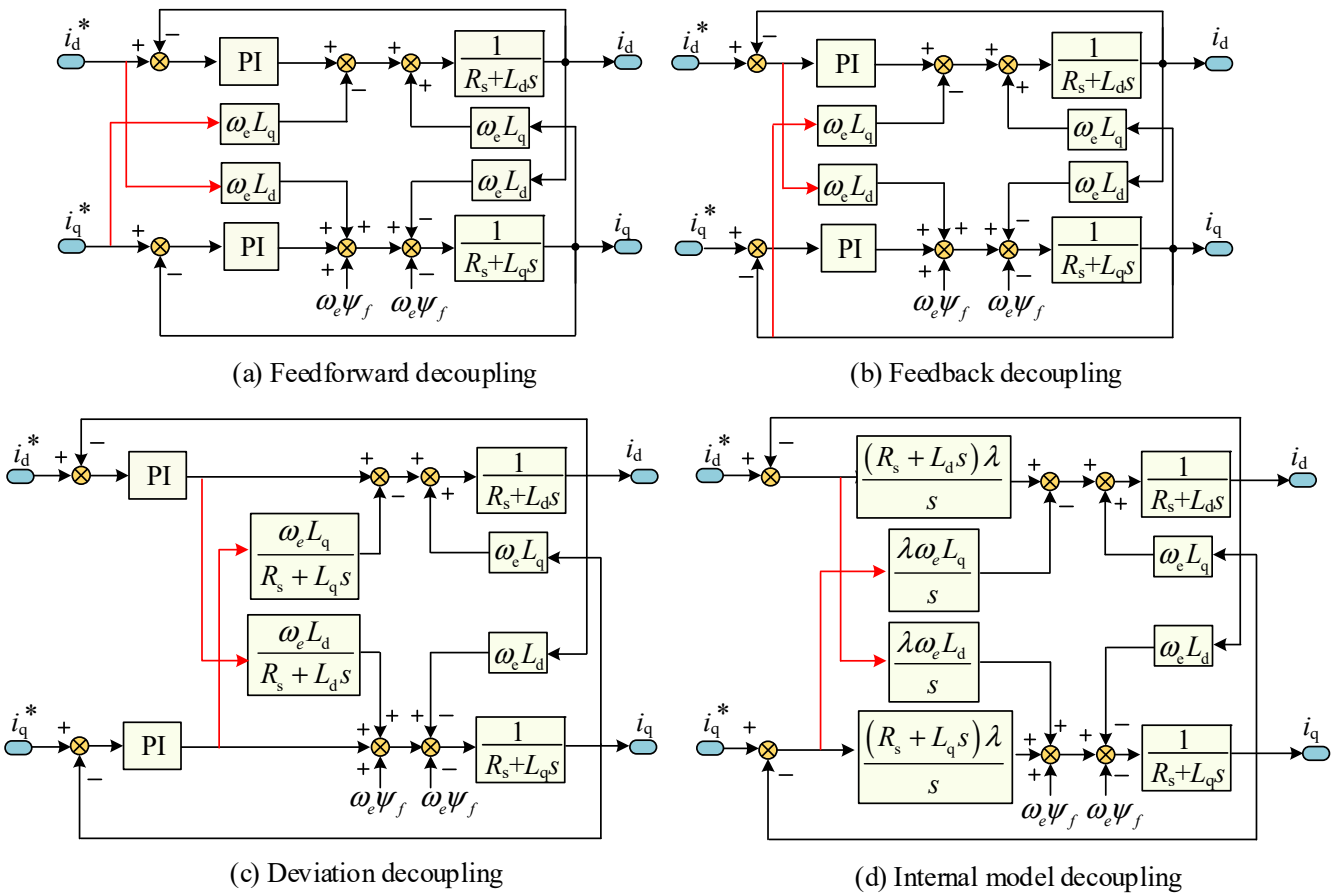
Under the condition of low carrier ratios, the coupling and delay mentioned above are more serious, which affects the stable operation of the HS PMM drive system. Non-coordinate transformation and decoupling control are two commonly used methods to solve the above problems. Among them, the non-coordinate transformation methods

include constant voltage frequency ratio control [78] and DTC [79]. The constant voltage frequency ratio control belongs to an open-loop control and has poor start and dynamic performances. As to the DTC, there is usually a serious torque ripple. Therefore, the above two methods are not suitable for HS PMM drives.

In the HS PMM control system, the most widely used decoupling control technology is based on a field-oriented control (FOC)strategy. Decoupling control strategies are mainly divided into two types: the decoupling control strategy based on scalars and the decoupling control strategy based on complex vectors.

5.3.1. Decoupling Control Strategy Based on Scalars

Decoupling control strategies based on scalars include feedforward decoupling [80], feedback decoupling [81], deviation decoupling [82], and internal model decoupling control technology [83]. The control block diagrams of feedforward decoupling and feedback decoupling are shown in Figure 9a and Figure 9b, respectively. The common point is that the coupling compensation term is superimposed after the current PI controllers. The given reference current is used in the feedforward decoupling control method, while the feedback current is used in the feedback decoupling control method. However, these two methods are sensitive to the motor parameters because they are based on the motor model. Therefore, it is difficult to achieve complete decoupling under parameter mismatches.



(a) Feedforward decoupling (b) Feedback decoupling

(c) Deviation decoupling (d) Internal model decoupling

Figure 9. Control block diagram of decoupling control strategies.

As shown in Figure 9c, the input of the compensation segment is moved behind the PI regulator; this method is called deviation decoupling. The internal model decoupling control technology is to move the input of the compensation segment to the front of the PI regulator, as shown in Figure 9d. The decoupling controllers based on the internal model

and deviation have preferable robustness to motor parameters, but they need to make a compromise between the decoupling effect and response.

5.3.2. Decoupling Control Strategy Based on Complex Vectors

The current loop PMSM model is a coupled multiple-input multiple-output (MIMO) system, which is difficult to analyze by the classical control theory. However, the complex vector is an effective method of analyzing the dynamic performance of symmetric MIMO systems [84]. The concept of complex vectors was proposed by P. K. Kovacs and I. Racz, and this method has been widely used in motor control systems [85].

The aim of the complex vector decoupling control strategy is to introduce complex zeros into the complex vector model of the motor so that they can be used to cancel the complex poles that vary with velocity. The following is the derivation process of the complex vector model. R_s stands for motor stator resistance; L_d and L_q represent the stator inductance of the dq axis; ω_e is the electric angular velocity; and u_{dq} and i_{dq} are the complex vector forms of voltage and current, respectively.

The complex vectors of current and voltage can be expressed as:

$$\begin{cases} u_{dq} = u_d + \mathrm{j}u_q \\ i_{dq} = i_d + ji_q \end{cases} \tag{2}$$

For the SPM, $L_d = L_q = L_s$, the voltage equation can be written as:

$$u_{dq} = R_s i_{dq} + sL_s i_{dq} + \mathrm{j}\omega_e L_s i_{dq} + \mathrm{j}\omega_e \psi_f \tag{3}$$

Considering the back EMF as the disturbance term, formula (3) can be expressed in the form of a transfer function as:

$$G_{dq}(s) = \frac{i_{dq}(s)}{u_{dq}(s)} = \frac{1}{L_s s + R_s + \mathrm{j}\omega_e L} \tag{4}$$

Thus, the current controller can be designed as:

$$u^*_{dq} = (K_p + \frac{K_i}{s} + \mathrm{j}\frac{K_p \omega_e}{s})(i^*_{dq} - i_{dq}) + \mathrm{j}\omega_e \psi_f \tag{5}$$

where K_p and K_i are the proportional coefficient and integral coefficient of the controller, respectively.

The above mathematical modeling is for the SPM. But for the IPM, L_d and L_q are not equal, so the IPM needs to be re-modeled. At present, the common method is the extended-back EMF method. In the dq frame, the complex vector model of the IPM based on extended-back EMF can be expressed as in (6).

$$u_{dq} = R_s i_{dq} + sL_d i_{dq} + \mathrm{j}\omega_e L_q i_{dq} + e_{dq} \tag{6}$$

where e_{dq} is the extended EMF vector and can be expressed as (7).

$$e_{dq} = \mathrm{j}[(L_d - L_q)(\omega_e i_d - s i_q) + \omega_e \psi_f] \tag{7}$$

The extended-back EMF is compensated by feedforward decoupling, and the controller design of the current loop is the same as the SPM.

The use of complex vectors to model and decouple the motor system has no essential difference from the use of scalars, except for the mathematical form, as shown in Figure 10. Since the digital microprocessor can only carry out scalar operations, the complex vector decoupling needs to be implemented in scalar forms.

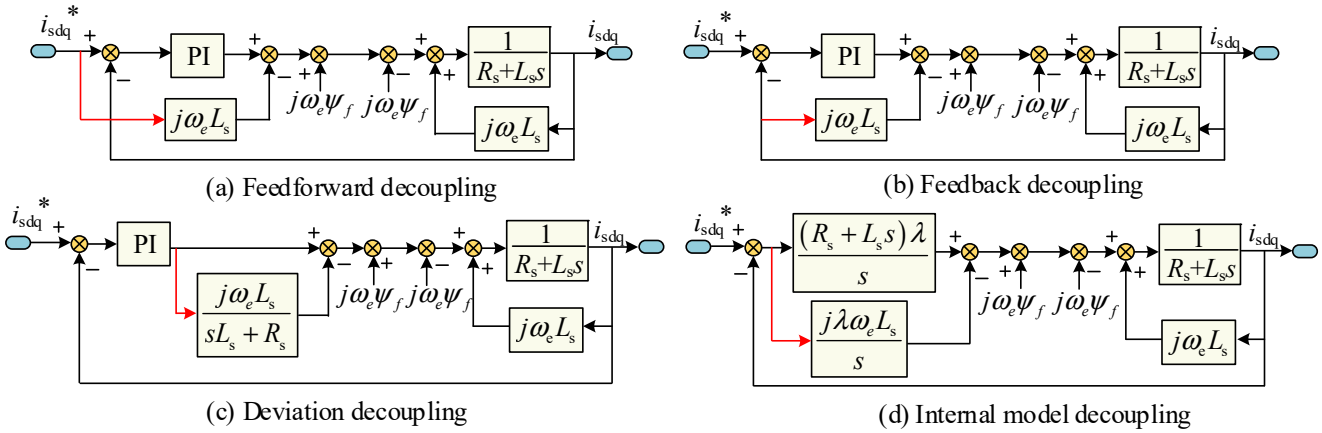


Figure 10. Diagram of complex vector decoupling control.

5.4. Compensation Strategies for Current Loop Delay

The coupling problem of HS PMMs is improved by the above control strategies, but the delay problem is still to be solved. At present, the delay compensation strategies can be divided into two kinds: model-based delay compensation strategies and model-independent delay compensation strategies.

5.4.1. Model-Based Delay Compensation Strategies

Model-based delay compensation strategies mainly include dynamic compensation, Smith estimator, and model predictive control. Due to the time-consuming calculation of the digital microprocessor, when the carrier ratio of the HS PMM drive is low, the delay time will produce serious phase and amplitude errors in the output voltage, which will affect the stability of the drive system. To solve this problem, a dynamic compensation strategy is proposed in [86]. The phase and amplitude errors are compensated by the PI regulator composed of the *dq* axis voltage difference between the delay and ideal states. The dynamic strategy is simple to calculate and the stability of the HS PMM drive system can be greatly improved.

To achieve delay-independent control in a system, a common solution is to use the Smith estimator. The PI speed controller is replaced by the Smith estimator, which has the ability to achieve superior control efficiency by eliminating the delay effect [87]. In [88], a model predictive current control strategy based on the Smith structure was introduced. The cost function was optimized and the Smith structure was used to compensate for the computation delay.

Compared with the above two methods, model predictive control (MPC) has the advantages of a simple design, fast dynamic response, and constant control frequency, so it has been widely considered. The MPC can be divided into a finite control set (FCS-MPC) and a continuous control set (CCS-MPC) [89,90]. The FCS-MPC mainly selects the optimal voltage vector as the control quantity by traversing all or part of the vectors in the vector set and combining them with specific value functions or optimization rules. The CCS-MPC usually combines the principle of deadbeat to solve the corresponding control quantity from the voltage equation.

5.4.2. Model-Independent Delay Compensation Strategies

Model-independent delay compensation strategies mainly include the linear prediction method [91] and the double sampling method [92,93]. The linear prediction method is suitable for the controlled system with strict linearization. However, when the permanent magnet motor works at a low carrier ratio, the nonlinearity of the system is more obvious.

The double-sampling strategy compensates for the delay in the algorithm execution. In [92], the mechanism of the digital control delay is analyzed, including computational delay and pulse width modulation delay. Then, based on two-stage and multi-stage phase

branches, a generalized real-time calculation method with dual-sampling mode is derived to directly eliminate the computation delay. Furthermore, in [93], a new calculation delay estimation and compensation technique based on double sampling within one control period are developed to reduce current and torque fluctuations.

6. Discussions and Future Research Trends

This article reviewed state-of-the-art driving technologies of the HS PMM. Although HS PMMs show promising advantages, many challenges exist in harmonic suppression, rotor position detection, and control strategies. Considering the practical implementation and application requirements, future development trends should focus on these aspects.

6.1. Control Performance of Current Loop with Low Carrier Ratios

The carrier ratio of HS PMM drive systems is low, resulting in the motor performance being significantly reduced. Therefore, improving the control performance of the current loop with low carrier ratios will draw more attention in the future.

6.2. High-Dynamic Performance of HS PMMs

HS PMM drive systems have digital control delay and serious current loop coupling, which seriously affects the dynamic performance of the system. From the perspective of the control strategy, it is important to improve the dynamic response ability of HS PMM drive systems.

6.3. Sensorless in Whole-Speed Range

The traditional sensorless position estimation method in the whole-speed range has two different position estimation methods at different speeds. These two position estimation methods need to be designed separately, which increases the difficulty of system tuning and the complexity of the algorithm. If sensorless control methods can estimate rotor position and speed with only one method in the whole-speed range, it will be more attractive for industrial applications.

6.4. Optimization of Inverter Topologies

As the main component of HS PMM drive systems, optimizing inverter topologies can not only improve the overall efficiency of the system but also reduce the volume of the filter inductor and capacitor on the basis of suppressing the current ripple, so as to improve the power density of the system.

7. Conclusions

In this article, the technical difficulties of HS PMM drives are analyzed, and the current research status is summarized from three aspects: harmonic suppression, rotor position estimation, and current control strategy:

(1) Due to the small inductor and high fundamental frequency of HS PMMs, the phase currents contain a large number of harmonics. In order to reduce the harmonic content, it is the most direct and effective scheme to increase the switching frequency of the system by using wide bandgap semiconductors. However, the additional power loss limits its application range. The main research direction for reducing harmonic content is to add the LCL filter and combine a new control algorithm with the system.
(2) In HS PMM drive systems, mechanical sensors are expensive and susceptible to harsh environments, so sensorless methods have been studied and applied. The SMO, the EKF, and the MRAS for estimating back EMFs have been widely accepted. Among them, the SMO-based sensorless control method has drawn increasing attention due to its simple implementation and strong robustness.
(3) The low carrier ratio of HS PMM drives causes coupling and delay increases. As to the coupling problem, feedforward decoupling and feedback decoupling are commonly used. However, these two decoupling methods are sensitive to the system parameters

and cannot be completely decoupled. The internal model decoupling control strategy in complex vector coordinate systems is the focus of the current research. For addressing the delay problem in the system, the predictive control strategy model based on the mathematical model is a common solution.

Funding: This research received no external funding.

Conflicts of Interest: The authors declare no conflict of interest.

References

1. Lee, C.-H.; Shin, H.-S.; Noh, H.-R.; Kim, K.-C. A Study on The Electromagnetic Multi-Step Transmission Characteristics of Interior Permanent Magnet Synchronous Motors. *Energies* **2022**, *15*, 9615. [CrossRef]
2. Arnaoutakis, G.E.; Kefala, G.; Dakanali, E.; Katsaprakakis, D.A. Combined Operation of Wind-Pumped Hydro Storage Plant with a Concentrating Solar Power Plant for Insular Systems: A Case Study for the Island of Rhodes. *Energies* **2022**, *15*, 6822. [CrossRef]
3. Zhang, F.; Du, G.; Wang, T.; Wang, F.; Cao, W.; Kirtley, J.L. Electromagnetic Design and Loss Calculations of a 1.12-MW High-Speed Permanent-Magnet Motor for Compressor Applications. *IEEE Trans. Energy Convers.* **2016**, *31*, 132–140. [CrossRef]
4. Cheng, M.; Li, Z.; Xu, S.; Pei, R. Design and Calculation of Multi-Physical Field of Ultra-High-Speed Permanent Magnet Motor. *Energies* **2024**, *17*, 3072. [CrossRef]
5. Garbiec, T.; Jagiela, M.; Kulik, M. Application of Nonlinear Complex Polyharmonic Finite-Element Models of High-Speed Solid-Rotor Induction Motors. *IEEE Trans. Magn.* **2020**, *56*, 7515304. [CrossRef]
6. Korkosz, M.; Bogusz, P.; Prokop, J. Complex Performance Analysis and Comparative Study of Very High-Speed Switched Reluctance Motors. *IEEE Trans. Magn.* **2019**, *55*, 8204714. [CrossRef]
7. Chen, Y.; Zang, B.; Wang, H.; Liu, H.; Li, H. Composite PM Rotor Design and Alternating Flux Density Harmonic Component Analysis of a 200 kW High-Speed PMSM Used in FESS. *IEEE Trans. Ind. Appl.* **2023**, *59*, 1469–1480. [CrossRef]
8. Binder, A.; Schneider, T.; Klohr, M. Fixation of buried and surface-mounted magnets in high-speed permanent-magnet synchronous machines. *IEEE Trans. Ind. Appl.* **2006**, *42*, 1031–1037. [CrossRef]
9. Baumgartner, T.; Burkart, R.M.; Kolar, J.W. Analysis and Design of a 300-W 500 000-r/min Slotless Self-Bearing Permanent-Magnet Motor. *IEEE Trans. Ind. Electron.* **2014**, *61*, 4326–4336. [CrossRef]
10. Jang, G.-H.; Ahn, J.-H.; Kim, B.-O.; Lee, D.-H.; Bang, J.-S.; Choi, J.-Y. Design and Characteristic Analysis of a High-Speed Permanent Magnet Synchronous Motor Considering the Mechanical Structure for High-Speed and High-Head Centrifugal Pumps. *IEEE Trans. Magn.* **2018**, *54*, 8204906. [CrossRef]
11. Zhang, F.; Du, G.; Wang, T.; Liu, G.; Cao, W. Rotor Retaining Sleeve Design for a 1.12-MW High-Speed PM Machine. *IEEE Trans. Ind. Appl.* **2015**, *51*, 3675–3685. [CrossRef]
12. Kong, Y.; Lin, M.; Jia, L. A Novel High Power Density Permanent-Magnet Synchronous Machine with Wide Speed Range. *IEEE Trans. Magn.* **2020**, *56*, 7505206. [CrossRef]
13. Dong, J.; Huang, Y.; Jin, L.; Lin, H. Comparative Study of Surface-Mounted and Interior Permanent-Magnet Motors for High-Speed Applications. *IEEE Trans. Appl. Supercond.* **2016**, *26*, 5200304. [CrossRef]
14. Wolnik, T.; Jarek, T. Solid Rotor Core vs. Lamination Rotor Core in Fractional-Slot PMSM Motor with High Power Density. *Energies* **2022**, *15*, 5729. [CrossRef]
15. Abubakar, U.; Wang, X.; Shah, S.H.; Wang, L.; Farouk, A. Electromagnetic and Thermal Analysis of 225 kW High-Speed PMSM for Centrifugal Blower Applications. *Energies* **2022**, *15*, 3370. [CrossRef]
16. Liang, Y.; Liang, D.; Jia, S.; Chu, S.; Wang, H.; Zhang, H.; Liang, Y. Compound Current Controller Based on SiC/Si Hybrid Converter for Current Harmonics Suppression of High-Speed PMSMs. *IEEE Trans. Ind. Appl.* **2023**, *59*, 6852–6867. [CrossRef]
17. Cao, X.; Ge, Q.; Wang, K.; Wang, Q.; Zheng, Y. High-speed Maglev Harmonic Current Suppression Strategy Based on Feedforward Compensation. In Proceedings of the 2021 24th International Conference on Electrical Machines and Systems (ICEMS), Gyeongju, Republic of Korea, 31 October–3 November 2021; pp. 1849–1853.
18. Bao, D.; Wu, H.; Wang, R.; Zhao, F.; Pan, X. Full-Order Sliding Mode Observer Based on Synchronous Frequency Tracking Filter for High-Speed Interior PMSM Sensorless Drives. *Energies* **2020**, *13*, 6511. [CrossRef]
19. Zhang, X.; Chen, Y.; Mollet, Y.; Yang, J.; Gyselinck, J. An Accurate Discrete Current Controller for High-Speed PMSMs/Gs in Flywheel Applications. *Energies* **2020**, *13*, 1458. [CrossRef]
20. Yuan, X.; Chen, J.; Jiang, C.; Lee, C.H.T. Discrete-Time Current Regulator for AC Machine Drives. *IEEE Trans. Power Electron.* **2022**, *37*, 5847–5858. [CrossRef]
21. Liu, X.; Liu, G.; Han, B. A Loss Separation Method of a High-Speed Magnetic Levitated PMSM Based on Drag System Experiment Without Torque Meter. *IEEE Trans. Ind. Electron.* **2019**, *66*, 2976–2986. [CrossRef]
22. Woo, J.-H.; Bang, T.-K.; Lee, H.-K.; Kim, K.-H.; Shin, S.-H.; Choi, J.-Y. Electromagnetic Characteristic Analysis of High-Speed Motors with Rare-Earth and Ferrite Permanent Magnets Considering Current Harmonics. *IEEE Trans. Magn.* **2021**, *57*, 8201805. [CrossRef]
23. Zhou, J.; Song, Z.; Xiao, X.; Huang, X.; Xie, Y. A Hybrid-Excited Resolver for High-Speed Operation. *IEEE Trans. Power Electron.* **2024**, *39*, 4958–4962. [CrossRef]

24. Tang, Q.; Shen, A.; Luo, X.; Xu, J. IPMSM Sensorless Control by Injecting Bidirectional Rotating HF Carrier Signals. *IEEE Trans. Power Electron.* **2018**, *33*, 10698–10707. [CrossRef]
25. Ye, M.; Shi, T.; Li, C.; Yan, Y.; Xia, C. High-Precision Sensorless Control of High-Speed Permanent Magnet Synchronous Motor Based on the Prediction Methodology. *IEEE Trans. Power Electron.* **2024**, *39*, 11386–11397. [CrossRef]
26. Sheianov, A.; Xiao, X.; Sun, X. An Enhanced Current Control Structure for Ultra-High-Speed Permanent Magnet Synchronous Motor Applications. *IEEE Trans. Ind. Appl.* **2024**, *60*, 4987–5001. [CrossRef]
27. Zhao, Y.; Deng, Z.; Ge, S. Research on Sensorless Technique of Ultra-High-Speed Permanent Magnet Synchronous Motor Considering Control Delays. In Proceedings of the 2023 26th International Conference on Electrical Machines and Systems (ICEMS), Zhuhai, China, 5–8 November 2023; pp. 2480–2485.
28. Velander, E.; Bohlin, G.; Sandberg, Å.; Wiik, T.; Botling, F.; Lindahl, M.; Zanuso, G.; Nee, H.P. An Ultralow Loss Inductorless dv/dt Filter Concept for Medium-Power Voltage Source Motor Drive Converters With SiC Devices. *IEEE Trans. Power Electron.* **2018**, *33*, 6072–6081. [CrossRef]
29. Kim, H.; Anurag, A.; Acharya, S.; Bhattacharya, S. Analytical Study of SiC MOSFET Based Inverter Output dv/dt Mitigation and Loss Comparison With a Passive dv/dt Filter for High Frequency Motor Drive Applications. *IEEE Access* **2021**, *9*, 15228–15238. [CrossRef]
30. Yao, Y.; Huang, Y.; Peng, F.; Dong, J.; Zhu, Z. Dynamic-Decoupled Active Damping Control Method for Improving Current Transient Behavior of LCL-Equipped High-Speed PMSMs. *IEEE Trans. Power Electron.* **2022**, *37*, 3259–3271. [CrossRef]
31. Zhou, J.; Yao, Y.; Huang, Y.; Peng, F. Motor Current Feedback-Only Active Damping Controller With High Robustness for LCL-Equipped High-Speed PMSM. *IEEE Trans. Power Electron.* **2023**, *38*, 8707–8718. [CrossRef]
32. Yao, Y.; Huang, Y.; Peng, F.; Dong, J.; Zhu, Z. Discrete-Time Dynamic-Decoupled Current Control for LCL-Equipped High-Speed Permanent Magnet Synchronous Machines. *IEEE Trans. Ind. Electron.* **2022**, *69*, 12414–12425. [CrossRef]
33. Ding, X.; Du, M.; Cheng, J.; Chen, F.; Ren, S.; Guo, H. Impact of Silicon Carbide Devices on the Dynamic Performance of Permanent Magnet Synchronous Motor Drive Systems for Electric Vehicles. *Energies* **2017**, *10*, 364. [CrossRef]
34. Do, T.V.; Li, K.; Trovão, J.P.; Boulon, L. Reviewing of Using Wide-bandgap Power Semiconductor Devices in Electric Vehicle Systems: From Component to System. In Proceedings of the 2020 IEEE Vehicle Power and Propulsion Conference (VPPC), Gijon, Spain, 18 November–16 December 2020; pp. 1–6.
35. Rogdakis, K.; Bano, E.; Montes, L.; Bechelany, M.; Cornu, D.; Zekentes, K. Rectifying Source and Drain Contacts for Effective Carrier Transport Modulation of Extremely Doped SiC Nanowire FETs. *IEEE Trans. Nanotechnol.* **2011**, *10*, 980–984. [CrossRef]
36. She, X.; Huang, A.Q.; Lucía, Ó.; Ozpineci, B. Review of Silicon Carbide Power Devices and Their Applications. *IEEE Trans. Ind. Electron.* **2017**, *64*, 8193–8205. [CrossRef]
37. Yuan, X.; Laird, I.; Walder, S. Opportunities, Challenges, and Potential Solutions in the Application of Fast-Switching SiC Power Devices and Converters. *IEEE Trans. Power Electron.* **2021**, *36*, 3925–3945. [CrossRef]
38. Lin, Z.; An, Q.; Xie, C. SiC-Based Inverter Fed High-Speed Permanent Magnet Synchronous Motor Drive. In Proceedings of the 2020 5th Asia Conference on Power and Electrical Engineering (ACPEE), Chengdu, China, 4–7 June 2020; pp. 1300–1304.
39. Morya, A.K.; Gardner, M.C.; Anvari, B.; Liu, L.; Yepes, A.G.; Doval-Gandoy, J.; Toliyat, H.A. Wide Bandgap Devices in AC Electric Drives: Opportunities and Challenges. *IEEE Trans. Transp. Electrif.* **2019**, *5*, 3–20. [CrossRef]
40. Zhang, B.; Wang, S. A Survey of EMI Research in Power Electronics Systems with Wide-Bandgap Semiconductor Devices. *IEEE J. Emerg. Sel. Top. Power Electron.* **2020**, *8*, 626–643. [CrossRef]
41. Guan, Q.X.; Li, C.; Zhang, Y.; Wang, S.; Xu, D.D.; Li, W.; Ma, H. An Extremely High Efficient Three-Level Active Neutral-Point-Clamped Converter Comprising SiC and Si Hybrid Power Stages. *IEEE Trans. Power Electron.* **2018**, *33*, 8341–8352. [CrossRef]
42. Cheng, Z.; Li, L.; Zhao, F.; Liu, J. Reduced-Order Extended Observer and Correction Discretization Method for High-Speed Permanent Magnet Synchronous Motor with LCL Filter. *IEEE J. Emerg. Sel. Top. Power Electron.* **2024**, *12*, 2831–2844. [CrossRef]
43. Wang, Z.; Li, X.; Xing, X.; Duan, B.; Zhang, C. Simultaneous Switching Loss Reduction and Neutral-Point Voltage Balance Scheme for Single-Phase Three-Level T-Type Inverter. *IEEE Trans. Ind. Appl.* **2020**, *56*, 6687–6700. [CrossRef]
44. Mathew, J.; Rajeevan, P.P.; Mathew, K.; Azeez, N.A.; Gopakumar, K. A Multilevel Inverter Scheme With Dodecagonal Voltage Space Vectors Based on Flying Capacitor Topology for Induction Motor Drives. *IEEE Trans. Power Electron.* **2013**, *28*, 516–525. [CrossRef]
45. Li, G.; Xu, S.; Sun, Z.; Yao, C.; Ren, G.; Ma, G. Open-Circuit Fault Diagnosis for Three-Level ANPC Inverter Based on Predictive Current Vector Residual. *IEEE Trans. Ind. Appl.* **2023**, *59*, 6837–6851. [CrossRef]
46. Ewanchuk, J.; Salmon, J.; Knight, A. Performance of a High Speed Motor Drive System Using a Novel Multi-Level Inverter Topology. In Proceedings of the 2008 IEEE Industry Applications Society Annual Meeting, Edmonton, AB, Canada, 5–9 October 2008; pp. 1–8.
47. Liu, Z.; Wang, Y.; Tan, G.; Li, H.; Zhang, Y. A Novel SVPWM Algorithm for Five-Level Active Neutral-Point-Clamped Converter. *IEEE Trans. Power Electron.* **2016**, *31*, 3859–3866. [CrossRef]
48. Wang, K.; Zheng, Z.; Wei, D.; Fan, B.; Li, Y. Topology and Capacitor Voltage Balancing Control of a Symmetrical Hybrid Nine-Level Inverter for High-Speed Motor Drives. *IEEE Trans. Ind. Appl.* **2017**, *53*, 5563–5572. [CrossRef]

49. Wu, H.; Huang, K.; Lv, W.; Mo, X.; Huang, S.; Zhou, J. DC-link Voltage Sliding Mode Control of Z-source Inverter for High Speed Permanent Magnet Motors. In Proceedings of the 2019 22nd International Conference on Electrical Machines and Systems (ICEMS), Harbin, China, 11–14 August 2019; pp. 1–6.
50. Gu, C.; Wang, X.; Shi, X.; Deng, Z. A PLL-Based Novel Commutation Correction Strategy for a High-Speed Brushless DC Motor Sensorless Drive System. *IEEE Trans. Ind. Electron.* **2018**, *65*, 3752–3762. [CrossRef]
51. Zhou, X.; Zhou, Y.; Peng, C.; Zeng, F.; Song, X. Sensorless BLDC Motor Commutation Point Detection and Phase Deviation Correction Method. *IEEE Trans. Power Electron.* **2019**, *34*, 5880–5892. [CrossRef]
52. Wang, Z.; Liu, J.; Cao, J.; Li, L.; Zhang, A.; Guo, Y. Research on High-speed Permanent Magnet Synchronous Motor Drive Based on PAM Method. In Proceedings of the 2023 26th International Conference on Electrical Machines and Systems (ICEMS), Zhuhai, China, 5–8 November 2023; pp. 2038–2042.
53. Migliazza, G.; Buticchi, G.; Carfagna, E.; Lorenzani, E.; Madonna, V.; Giangrande, P.; Galea, M. DC Current Control for a Single-Stage Current Source Inverter in Motor Drive Application. *IEEE Trans. Power Electron.* **2021**, *36*, 3367–3376. [CrossRef]
54. Wu, Y.; Lu, Y.; Li, S.; An, Q. Active Disturbance Rejection Control Based Deadbeat Predictive Current Controller for CSI-Fed SPMSM Systems. In Proceedings of the 2024 IEEE 10th International Power Electronics and Motion Control Conference (IPEMC2024-ECCE Asia), Chengdu, China, 10 July 2024; pp. 2559–2563.
55. Feng, W.; Ding, H.; Chen, F.; Lee, S.; Chen, K.; Jahns, T.; Sarlioglu, B. Design of High Power Density 100 kW Surface Permanent Magnet Machine with No Heavy Rare Earth Material Using Current Source Inverter for Traction Application. In Proceedings of the 2021 IEEE Transportation Electrification Conference & Expo (ITEC), Chicago, IL, USA, 21–25 June 2021; pp. 1–6.
56. Jiang, D.; Xiong, Y.; Liu, K.; Liu, Z.; Wang, R.; Yang, K. Common Mode Suppression Method of Current Source Back-to-Back Converter Based on Five-Segment Space Vector Modulation. *IEEE Trans. Ind. Appl.* **2023**, *59*, 1035–1043. [CrossRef]
57. Wei, Q.; Xing, L.; Xu, D.; Wu, B.; Zargari, N.R. Modulation Schemes for Medium-Voltage PWM Current Source Converter-Based Drives: An Overview. *IEEE J. Emerg. Sel. Top. Power Electron.* **2019**, *7*, 1152–1161. [CrossRef]
58. Liu, P.; Wang, Z.; Xu, Y.; Zou, Z.; Deng, F.; Li, Y. Improved Harmonic Profile for High-Power PWM Current-Source Converters With Modified Space-Vector Modulation Schemes. *IEEE Trans. Power Electron.* **2021**, *36*, 11234–11244. [CrossRef]
59. Yang, S.; Yin, Z.; Tong, C.; Sui, Y.; Zheng, P. Active Damping Current Control for Current-Source Inverter-Based PMSM Drives. *IEEE Trans. Ind. Electron.* **2023**, *70*, 3549–3560. [CrossRef]
60. Lee, H.-J.; Jung, S.; Sul, S.-K. A Current Controller Design for Current Source Inverter-Fed AC Machine Drive System. *IEEE Trans. Power Electron.* **2023**, *28*, 1366–1381. [CrossRef]
61. Chen, S.; Zhao, Y.; Qiu, H.; Ren, X. High-Precision Rotor Position Correction Strategy for High-Speed Permanent Magnet Synchronous Motor Based on Resolver. *IEEE Trans. Power Electron.* **2020**, *35*, 9716–9726. [CrossRef]
62. Wang, Y.; Bao, X.; Hua, W.; Liu, K.; Wang, P.; Hu, M.; Zhang, H. Implementation of Embedded Magnetic Encoder for Rotor Position Detection Based on Arbitrary Phase-Shift Phase-Lock Loop. *IEEE Trans. Ind. Electron.* **2022**, *69*, 2033–2043. [CrossRef]
63. Miguel-Espinar, C.; Heredero-Peris, D.; Igor-Gross, G.; Llonch-Masachs, M.; Montesinos-Miracle, D. Accurate Angle Representation From Misplaced Hall-Effect Switch Sensors for Low-Cost Electric Vehicle Applications. *IEEE Trans. Ind. Appl.* **2022**, *58*, 5227–5237. [CrossRef]
64. Wang, Y.; Liu, K.; Hua, W.; Zhang, C.; Wu, Z.; Zhang, H. Analysis and Detection of Rotor Eccentricity in Permanent Magnet Synchronous Machines Based on Linear Hall Sensors. *IEEE Trans. Power Electron.* **2022**, *37*, 4719–4729. [CrossRef]
65. Song, X.; Fang, J.; Han, B. High-Precision Rotor Position Detection for High-Speed Surface PMSM Drive Based on Linear Hall-Effect Sensors. *IEEE Trans. Power Electron.* **2016**, *31*, 4720–4731.
66. Wang, G.; Yang, R.; Xu, D. DSP-Based Control of Sensorless IPMSM Drives for Wide-Speed-Range Operation. *IEEE Trans. Ind. Electron.* **2013**, *60*, 720–727. [CrossRef]
67. Huang, M.C.; Moses, A.J.; Anayi, F.J.; Yao, X.G. Shaft Position Correction Scheme Comparison for Sensorless Control PMSM based on Space State-Estimation between α-β Variance Adjustment and d-q Angle PI Regulation. In Proceedings of the IECON 2006—32nd Annual Conference on IEEE Industrial Electronics, Paris, France, 7–10 November 2006; pp. 1469–1474.
68. Accetta, A.; Cirrincione, M.; Pucci, M.; Vitale, G. Neural Sensorless Control of Linear Induction Motors by a Full-Order Luenberger Observer Considering the End Effects. *IEEE Trans. Ind. Appl.* **2014**, *50*, 1891–1904. [CrossRef]
69. Qiao, Z.; Shi, T.; Wang, Y.; Yan, Y.; Xia, C.; He, X. New Sliding-Mode Observer for Position Sensorless Control of Permanent-Magnet Synchronous Motor. *IEEE Trans. Ind. Electron.* **2013**, *60*, 710–719. [CrossRef]
70. Feng, Y.; Yu, X.; Han, F. High-Order Terminal Sliding-Mode Observer for Parameter Estimation of a Permanent-Magnet Synchronous Motor. *IEEE Trans. Ind. Electron.* **2013**, *60*, 4272–4280. [CrossRef]
71. An, Q.; Zhang, J.; An, Q.; Liu, X.; Shamekov, A.; Bi, K. Frequency-Adaptive Complex-Coefficient Filter-Based Enhanced Sliding Mode Observer for Sensorless Control of Permanent Magnet Synchronous Motor Drives. *IEEE Trans. Ind. Appl.* **2020**, *56*, 335–343. [CrossRef]
72. Quang, N.K.; Hieu, N.T.; Ha, Q.P. FPGA-Based Sensorless PMSM Speed Control Using Reduced-Order Extended Kalman Filters. *IEEE Trans. Ind. Electron.* **2014**, *61*, 6574–6582. [CrossRef]
73. Quang, N.K.; Tung, D.D.; Ha, Q.P. FPGA-based sensorless PMSM speed control using adaptive extended Kalman filter. In Proceedings of the 2015 IEEE International Conference on Automation Science and Engineering (CASE), Gothenburg, Sweden, 24–28 August 2015; pp. 1650–1655.

74. Wei, F.; Wang, Y.; Liang, Q.; Li, Z. Sensorless Control of Permanent Magnet Synchronous Motor Based on Improved Model Reference Adaptive System. In Proceedings of the 2019 Chinese Automation Congress (CAC), Hangzhou, China, 22–24 November 2019; pp. 2422–2426.
75. Liu, Y.; Zhu, Z.Q.; Howe, D. Commutation-Torque-Ripple Minimization in Direct-Torque-Controlled PM Brushless DC Drives. *IEEE Trans. Ind. Appl.* **2007**, *43*, 1012–1021. [CrossRef]
76. Masmoudi, M.; Badsi, B.E.; Masmoudi, A. DTC of B4-Inverter-Fed BLDC Motor Drives with Reduced Torque Ripple During Sector-to-Sector Commutations. *IEEE Trans. Power Electron.* **2014**, *29*, 4855–4865. [CrossRef]
77. Lee, K.-W.; Park, S.; Jeong, S. A Seamless Transition Control of Sensorless PMSM Compressor Drives for Improving Efficiency Based on a Dual-Mode Operation. *IEEE Trans. Power Electron.* **2015**, *30*, 1446–1456. [CrossRef]
78. Itoh, J.-I.; Toi, T.; Nishizawa, K. Stabilization Method Using Equivalent Resistance Gain Based on V/f Control for IPMSM with Long Electrical Time Constant. In Proceedings of the 2018 International Power Electronics Conference (IPEC-Niigata 2018-ECCE Asia), Niigata, Japan, 20–24 May 2018; pp. 2229–2236.
79. Yoshimoto, J.; Inoue, Y.; Morimoto, S.; Sanada, M. Ultra-high-speed PMSM sensorless drive using direct torque control. In Proceedings of the 2012 15th International Conference on Electrical Machines and Systems (ICEMS), Sapporo, Japan, 21–24 October 2012; pp. 1–6.
80. Zhou, S.; Zhang, Y.; Liu, Z.; Liu, J.; Zhou, L. Implementation of Cross-Coupling Terms in Proportional-Resonant Current Control Schemes for Improving Current Tracking Performance. *IEEE Trans. Power Electron.* **2021**, *36*, 13248–13260. [CrossRef]
81. Zhang, Z.; Jing, L.; Wu, X.; Xu, W.; Liu, J.; Lyu, G.; Fan, Z. A Deadbeat PI Controller With Modified Feedforward for PMSM Under Low Carrier Ratio. *IEEE Access* **2021**, *9*, 63463–63474. [CrossRef]
82. Zhihong, W.; Shuangquan, W.; Yuan, Z.; Guangyu, T. Research on discrete deviation decoupling control for permanent magnet synchronous motor. In Proceedings of the 2010 International Conference on Computer Application and System Modeling (ICCASM 2010), Taiyuan, China, 22–24 October 2010; pp. V3-428–V3-431.
83. Lyu, Z.; Wu, L. Current Control Scheme for LC-Equipped PMSM Drive Considering Decoupling and Resonance Suppression in Synchronous Complex-Vector Frame. *IEEE J. Emerg. Sel. Top. Power Electron.* **2023**, *11*, 2061–2073. [CrossRef]
84. Chen, F.; Chen, Z.; Li, Z.; Huang, X.; Zhang, J. An Improved Complex Vector Decoupling Control for high-speed PMSM. In Proceedings of the 2021 IEEE International Electric Machines & Drives Conference (IEMDC), Hartford, CT, USA, 17–20 May 2021; pp. 1–6.
85. Huh, K.-K.; Lorenz, R.D. Discrete-Time Domain Modeling and Design for AC Machine Current Regulation. In Proceedings of the 2007 IEEE Industry Applications Annual Meeting, New Orleans, LA, USA, 23–27 September 2007; pp. 2066–2073.
86. Lv, W.; Huang, K.; Wu, H.; MO, X.; Shen, M. A Dynamic Compensation Method for Time Delay Effects of High-Speed PMSM Sensorless Digital Drive System. In Proceedings of the 2019 22nd International Conference on Electrical Machines and Systems (ICEMS), Harbin, China, 11–14 August 2019; pp. 1–5.
87. Nicola, M.; Nicola, C.-I.; Duță, M. Delay Compensation in the PMSM Control by using a Smith Predictor. In Proceedings of the 2019 8th International Conference on Modern Power Systems (MPS), Cluj-Napoca, Cluj, Romania, 21–23 May 2019; pp. 1–6.
88. Wei, Y.; Wei, Y.; Sun, Y.; Qi, H.; Guo, X.; Li, M. A Smith Structure-Based Delay Compensation Method for Model Predictive Current Control of PMSM System. *IEEE J. Emerg. Sel. Top. Power Electron.* **2022**, *10*, 4090–4101. [CrossRef]
89. Zhang, Y.; Xu, D.; Huang, L. Generalized Multiple-Vector-Based Model Predictive Control for PMSM Drives. *IEEE Trans. Ind. Electron.* **2018**, *65*, 9356–9366. [CrossRef]
90. Xiao, M.; Shi, T.; Yan, Y.; Xu, W.; Xia, C. Predictive Torque Control of Permanent Magnet Synchronous Motors Using Flux Vector. *IEEE Trans. Ind. Appl.* **2018**, *54*, 4437–4446. [CrossRef]
91. Lee, M.; Kong, K. Fourier-Series-Based Phase Delay Compensation of Brushless DC Motor Systems. *IEEE Trans. Power Electron.* **2018**, *33*, 525–534. [CrossRef]
92. Lin, Z.; Ruan, X.; Zhang, H.; Wu, L. A Generalized Real-Time Computation Method with Dual-Sampling Mode to Eliminate the Computation Delay in Digitally Controlled Inverters. *IEEE Trans. Power Electron.* **2022**, *37*, 5186–5195. [CrossRef]
93. Han, Y.; Gong, C.; Yan, L.; Wen, H.; Wang, Y.; Shen, K. Multiobjective Finite Control Set Model Predictive Control Using Novel Delay Compensation Technique for PMSM. *IEEE Trans. Power Electron.* **2020**, *35*, 11193–11204. [CrossRef]

Disclaimer/Publisher's Note: The statements, opinions and data contained in all publications are solely those of the individual author(s) and contributor(s) and not of MDPI and/or the editor(s). MDPI and/or the editor(s) disclaim responsibility for any injury to people or property resulting from any ideas, methods, instructions or products referred to in the content.